




# High axial resolution and long field of view for light-sheet fluorescence microscopy via double-beam aperture

L. V. Nhu<sup>1,2,a</sup> , Xuanhoi Hoang<sup>2</sup>, Minhnggia Pham<sup>2</sup>, Hoanghai Le<sup>2</sup>

<sup>1</sup> Institute of Research and Development, Duy Tan University, Da Nang 550000, Vietnam

<sup>2</sup> Le Quy Don Technical University, Hanoi 100000, Vietnam

Received: 15 November 2019 / Accepted: 19 April 2020

© Società Italiana di Fisica and Springer-Verlag GmbH Germany, part of Springer Nature 2020

**Abstract** We propose a simple method based on the use of interference of the double-beam aperture to enhance both the axial resolution and field of view of light-sheet fluorescence microscopy. The double-beam aperture placed in the pupil plane generates multiple-spot intensity patterns in which the size of central lobe reduces. By scanning this intensity pattern along  $x$ -axis, the light sheet is generated. By satisfactorily choosing the numerical apertures of illumination lens and detection lens, only the central light sheet is used to achieve image, so the axial resolution of light-sheet fluorescence microscopy is enhanced. Both the numerical apertures of the illumination lens and detection lens of 0.3 and 1.1, respectively, are employed to perform the simulation results. The simulation results indicated that both the axial resolution and field of view are improved in comparison to the Gaussian light-sheet. Additionally, in order to remove a small amount of the existing outside lobes, we propose a subtraction method. The simulation results demonstrated that our technique can eliminate the outside lobes in the system point spread function of the double-beam aperture beam light sheet.

## 1 Introduction

Three-dimensional (3D) dynamic fluorescence imaging is estimable for a better understanding of the biological processes. There are some techniques for obtaining 3D images introduced, such as confocal scanning fluorescence microscopy, light-sheet fluorescence microscopy and wide-field fluorescence microscopy. However, these techniques have the challenging in 3D dynamic imaging with the subcellular spatial resolution because the 3D dynamic imaging requires a satisfactory balance between some requirements including the spatial resolution, the optical sectioning, the imaging speed and both photo-bleaching and photo-damage. Light-sheet fluorescence microscopy was firstly introduced by Siedentopf and Zsigmondy [1]. The first 3D imaging application of the light-sheet fluorescence microscopy is shown by Voie et al. [2], and it was subsequently developed by Stelzer et al. [3]. For the development of light-sheet fluorescence microscopy, many variants have been reported [4–10]. Recently, this technique can be combined with other techniques, such as individual

<sup>a</sup> e-mail: [levannhu\\_mta2013@yahoo.com](mailto:levannhu_mta2013@yahoo.com) (corresponding author)

molecule localization [11], SIM [12], STED [13] and subtraction method [14], to enhance the axial resolution.

There are two fundamental ways to generate the light-sheet beam. In the first way, when a collimated laser beam goes through a cylindrical lens, the light sheet is generated. This light sheet was called the static light-sheet beam, so the complete light sheet is instantaneously formed. This light sheet is employed popularly because it generates simply. Another way, when a collimated laser beam passes through an objective lens, the thin laser beam is generated. Then, the light sheet generated by this laser beam is fast scanned by the use of a galvo mirror over the field of view. This light sheet was called the virtual light-sheet beam.

The axial resolution of light-sheet fluorescence microscopy is determined by the thickness of the light sheet. Many researchers focused to create thinner light sheets in comparison with the Gaussian light sheet. On a conventional light-sheet fluorescence microscopy setup, for the specified numerical apertures (NAs) of the illumination lens and the objective lens, the width of the light-sheet waist is determined. In order to generate longer and thinner light sheets, some methods using special light beams, such as Bessel beams [15] and Airy beams [16], have also been introduced in light-sheet fluorescence microscopy. Moreover, the STED method is also applied for the improvement in the axial resolution. The way has been implemented by overlapping between the Gaussian excitation light sheet and the STED light sheet [17]. However, the scattering and possibly additional aberrations which are caused by the wavelength difference between excitation and STED light will limit the maximal acquirable resolution in biological specimens. Recently, the method to generate light sheets via interference of beams has been introduced [18–20]. The authors introduced six beams to generate the light sheets [19, 20]. In other research, they have introduced a slit to generate light sheets [18]. In all these papers, the NAs of the illumination and detection lenses are suitably chosen, to reduce the effectiveness of the outside lobes of the system point spread function (PSF). In this paper, we propose a simple method based on the use of interference of the double-beam aperture to enhance both the axial resolution and the field of view in light-sheet fluorescence microscopy. This method but also does not change the setup of the optical system, can be easily performed. Moreover, we also introduce additionally the subtraction method to remove the outside lobes of the PSF. By using the method, the outside lobes do not present in the system PSF. This means that the gap in the optical transfer function can be avoided.

## 2 Illumination beam with double-beam aperture

We introduce two wave planes by employing double-beam aperture as shown in Fig. 1b. With this double-beam aperture, two wave planes will be interfered and therefore the size of the central core of the intensity distribution is reduced in comparison with the size of the intensity distribution of Gaussian beam. By choosing the satisfactory NAs of illumination lens and detection lens, only the central core of the intensity distribution of the double-beam aperture beam is employed to achieve image, while the others of the intensity distribution are removed. This means that the axial resolution with the double-beam aperture beam is improved in comparison with the Gaussian beam.

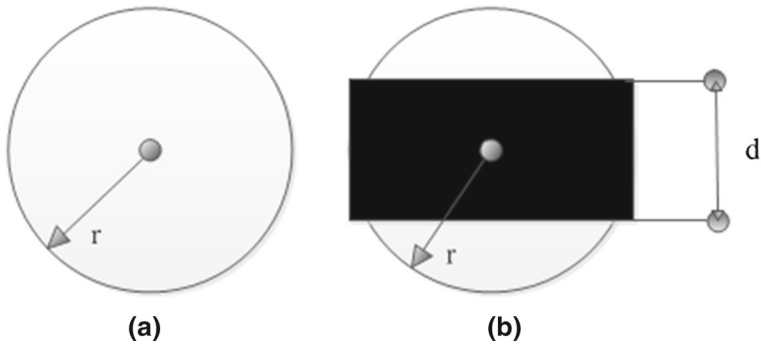


**Fig. 1** The aperture shape of **a** the Gaussian beam and **b** the double-beam aperture beam

Based on the use of vectorial diffraction theory, the spatial distribution of incident light propagated through one objective lens can be determined. By using the formulae explicitly derived by the Debye integral, the electric field in near the focus can be calculated by Eq. (1):

$$\vec{E}(r_2, \varphi_2, z_2) = iC \iint_{\Omega} \sin(\theta) E_0 A(\theta, \varphi) P \times e^{i\Delta a(\theta, \varphi)} e^{ikn(z_2 \cos \theta + r_2 \sin \theta \cos(\varphi - \varphi_2))} d\theta d\varphi \tag{1}$$

where  $\vec{E}(r_2, \varphi_2, z_2)$  denotes the electric field vector at the given point,  $(r_2, \varphi_2, z_2)$  present in cylindrical coordinates,  $C$  denotes the normalized constant,  $E_0$  denotes the amplitude function of the incident light,  $A(\theta, \varphi)$  denotes a  $3 \times 3$  matrix related to the structure of the imaging lens and  $P$  denotes Jose’s vector of the incident light.  $\Delta a(\theta, \varphi)$  is the parameter of phase delay produced by the phase mask.

When the objective lens satisfies with the sine condition,  $A(\theta, \varphi)$  can be presented as,

$$A(\theta, \varphi) = \sqrt{\cos \theta} \begin{bmatrix} 1 + (\cos \theta - 1) \cos^2 \varphi & (\cos \theta - 1) \cos \varphi \sin \varphi & -\sin \theta \cos \varphi \\ (\cos \theta - 1) \cos \varphi \sin \varphi & 1 + (\cos \theta - 1) \sin^2 \varphi & -\sin \theta \sin \varphi \\ \sin \theta \cos \varphi & \sin \theta \sin \varphi & \cos \theta \end{bmatrix}. \tag{2}$$

In this paper, the  $NA$  value of the illumination lens,  $NA = 0.3$ , is chosen to demonstrate the effective ability of the proposed method. The calculation results of the PSFs with different sizes for the double-beam aperture are depicted in Fig. 2, where  $d/(2*r)$  value is set to 0.2, 0.4, 0.6 and 0.8. It is not difficult to see that the shape of PSF depends on the ratio of  $d/(2*r)$  value. When the  $d/(2*r)$  value is increased, the outside lobes are also increased. However, the size of the central core of the intensity distribution along  $z$ -axis is decreased.

### 3 Imaging performance of light-sheet fluorescence microscopy with the double-beam aperture

In this paper, the illumination  $NA$  of  $NA = 0.3$  is used to demonstrate the effectiveness of the proposed method. The double-beam aperture is chosen with the size of  $d/(2*r) = 0.5$ . By using Eq. (1), the intensity distributions of the Gaussian beam and the double-beam aperture beam in the  $xz$ -plane are plotted in Fig. 3. As Fig. 3 indicates, the intensity distribution of the double-beam aperture includes one central lobe and the outside lobes. It can be seen from Fig. 3 that the size of the Gaussian beam is bigger than that of the central core of the double-beam aperture beam. As we have known that the thickness of the light sheet and the

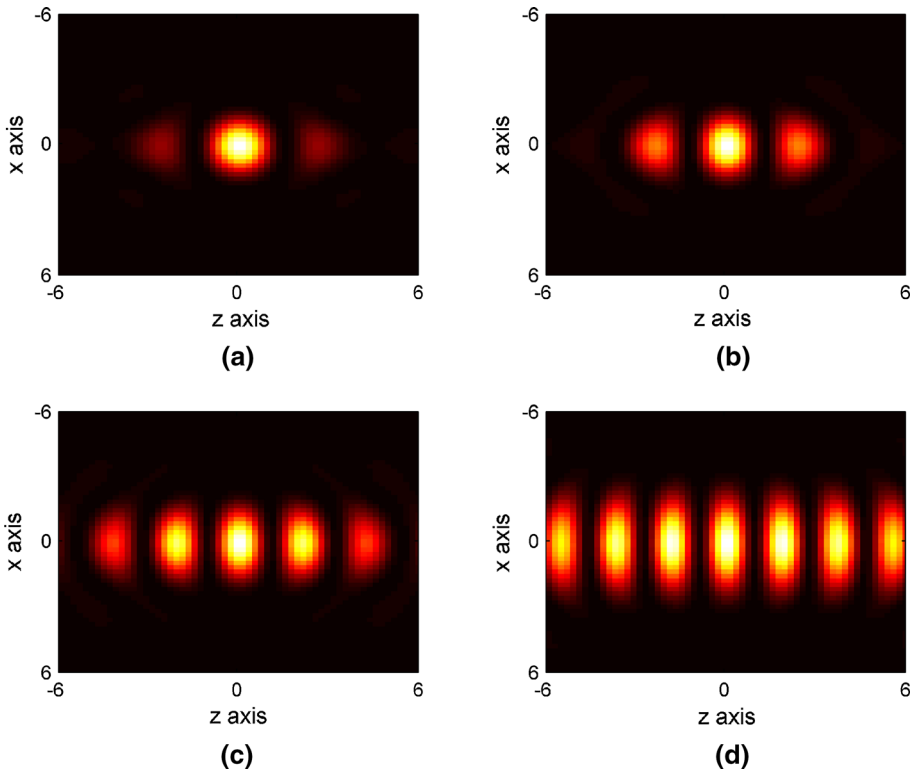


**Fig. 2** The PSFs with different sizes of the double-beam aperture: **a**  $d/(2*r) = 0.2$ ; **b**  $d/(2*r) = 0.4$ ; **c**  $d/(2*r) = 0.6$  and **d**  $d/(2*r) = 0.8$ . The unit along these axes is the wavelength

axial resolution of the detection lens can be employed to determine the axial resolution of the light sheet. When the axial resolution of the detection lens is bigger than the thickness of the light-sheet, the thickness of the light-sheet will mainly decide the axial resolution of light-sheet fluorescence microscopy. In order to achieve high axial resolution of light-sheet fluorescence microscopy with the double-beam aperture beam, the  $NA$  value of detection lens should be chosen suitably to eliminate the outside lobes. Then, the thickness of the central lobe will decide the axial resolution of light sheet. By simulation process, we found that the  $NA$  value of the detection part,  $NA = 1.1$ , is adequate.

In order to judge the ability to extend the field of view of the proposed method, the intensity distributions of the Gaussian and double-beam aperture beams in  $yz$ -plane are indicated in Fig. 4. As mentioned, the central intensity distribution of the double-beam aperture beam is used to obtain the image, so the light-sheet length of the double-beam aperture beam will be determined by the central intensity. From Fig. 4, it can be seen that the light-sheet length of the double-beam aperture is longer than that of the Gaussian beam. In order to show the light-sheet length of these two beams, the normalized central peak intensity of these intensity distributions along  $y$ -axis is depicted in Fig. 5. We use the intensity level of 0.5 to show the effective length of the light sheets. The length of the light sheet of the double-beam aperture is longer about 1.4 times than that of the Gaussian light sheet.

Herein, we will use the second way to generate the light sheet. When the intensity distributions of both the Gaussian beam and the double-beam aperture beam are fast scanned

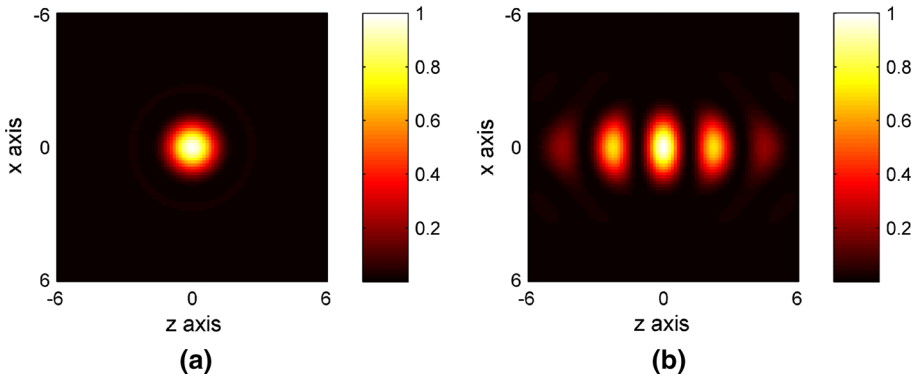


**Fig. 3** The intensity distributions: **a** the Gaussian beam in the  $xz$ -plane and **b** the double-beam aperture beam in the  $xz$ -plane. The unit along these axes is the wavelength

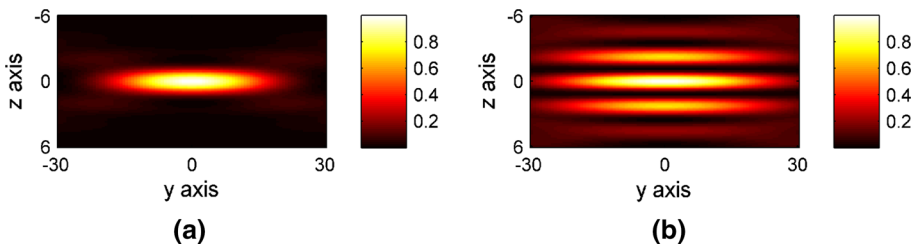


**Fig. 4** The intensity distributions of two beams: **a** Gaussian beam and **b** double-beam aperture beam in the  $yz$ -plane. The unit along these axes is the wavelength

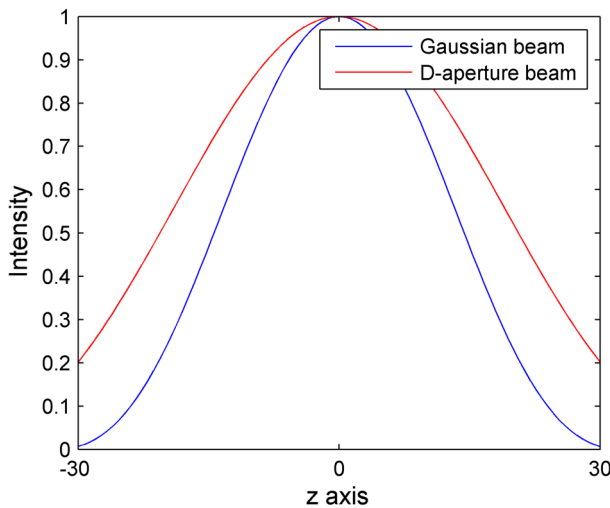


**Fig. 5** The intensity distribution of the Gaussian beam and the double-beam aperture beam on  $y$ -axis. The unit along these axes is the wavelength

along  $x$ -axis, both light sheets are generated. Figure 6 plots the cross sections of the intensity distributions of both the Gaussian light sheet and the double-beam aperture light sheet in

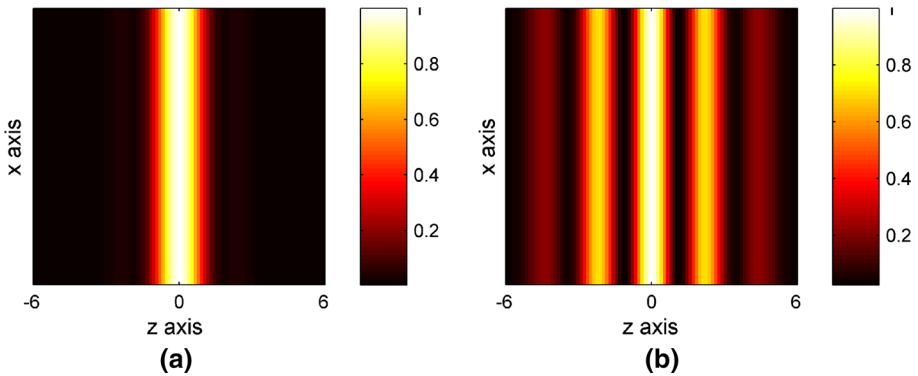


**Fig. 6** The intensity distributions of two light sheets: **a** Gaussian light sheet and **b** double-beam aperture light sheet. The unit along these axes is the wavelength

$xz$ -plane. For the double-beam aperture light sheet, the inside lobe will be used to acquire the image, while the impact of the outside lobes will be eliminated. Therefore, the thickness of the double-beam light sheet is decided by the size of the central light sheet. We use full width at half maximum (FWHM) to compare the width between the central light sheet and the Gaussian light sheet. The width of the central light sheet is smaller a factor of 1.3 times than one of the Gaussian light sheets.

In order to demonstrate the effectiveness of the proposed method for the enhancement of the axial resolution, we will evaluate the system PSF of light-sheet fluorescence microscopy. The system PSF for light-sheet fluorescence microscopy can be calculated by multiplying the illumination PSF with the detection PSF and can be described by,

$$\text{PSF}_{\text{system}}(x, y, z) = \text{PSF}_{\text{Illu}}(x, y, z) \times \text{PSF}_{\text{Detec}}(x, y, z) \quad (3)$$

where  $\text{PSF}_{\text{system}}$  denotes the system PSF,  $\text{PSF}_{\text{Illu}}$  is the illumination PSF and  $\text{PSF}_{\text{Detec}}$  denotes the detection PSF.

Now, we use Eq. (3) to simulate the system PSFs of the two light sheets. The system PSF of the Gaussian light sheet in  $zx$ -plane is shown in Fig. 7a. Figure 7b presents the system PSF of the double-beam aperture light sheet. It is not difficult to see that the system PSF of the double-beam aperture beam light sheet along  $z$ -optical axis is smaller than that of the conventional light-sheet fluorescence microscopy. In other words, the axial resolution of the double-beam aperture beam light sheet is higher than that of the conventional light-sheet fluorescence microscopy. In order to highlight the proposed method for the improvement in the axial resolution, Fig. 8 shows the intensity distributions of the two system PSFs of the double-beam aperture beam and the conventional light-sheet fluorescence microscopy along  $z$ -optical axis. The axial resolution of the double-beam aperture light sheet is better about 1.2 times than that of the Gaussian light sheet.

The optical transfer function (OTF) is equal to the Fourier transform,  $FFT$ , of the PSF and can be presented by,

$$\text{OTF}(f_x, f_y, f_z) = \text{FFT}\{\text{PSF}(x, y, z)\} \quad (4)$$

where OTF is the optical transfer function of the imaging system and  $f_x$ ,  $f_y$  and  $f_z$  are the spatial frequencies.

Figure 9 shows the system PSF and the MTF in  $zx$ -plane. As can be seen from Fig. 9a, the outside lobes of the system PSF in  $z$ -direction still have a small amount of intensity

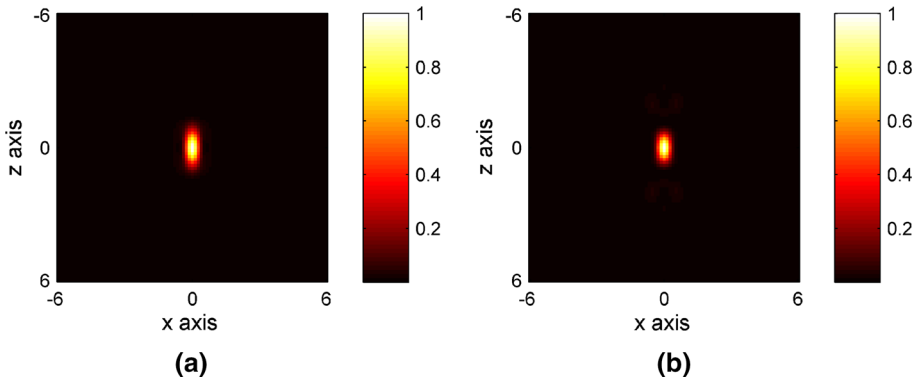


**Fig. 7** The system PSFs for two light sheets: **a** the system PSF with the conventional light-sheet fluorescence microscopy in  $xz$ -plane; **b** the system PSF with double-beam aperture beam light sheet. The unit along these axes is the wavelength

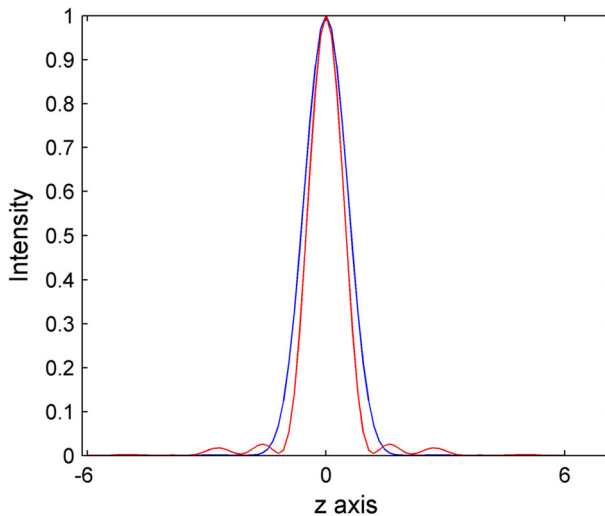


**Fig. 8** The cross section of the intensity distribution of the Gaussian beam light sheet (blue line) and double-beam aperture beam light sheet (red line) along  $z$ -axis. The unit along the axis is the wavelength

distributions. This will generate the OTF that has gaps. In order to show clearly this problem, the MTF in  $xz$ -plane is depicted in Fig. 9b. It is not difficult to see that there are additionally two peaks on the MTF in  $xz$ -plane. This will lead the gaps on the OTF along  $z$ -direction.

Next, the aim of us is to seek the method for the reduction in gaps on the OTF. In order to deal with the problem, we find a method to eliminate the outside lobes in the system PSF of the double-beam aperture beam light sheet. An effective method for the reduction of background is the subtraction method [21, 22]. In this paper, we will use the subtraction method to reduce the outside lobes in the system PSF of the double-beam aperture beam light sheet. The subtraction method includes two imaging processes with two illumination paths: The first path is the double-beam aperture beam and the second path is the doughnut one. The second doughnut PSF is modulated by the phase mask. Moreover, the phase mask is inserted in the optical system of the double-beam aperture beam light sheet. For light-

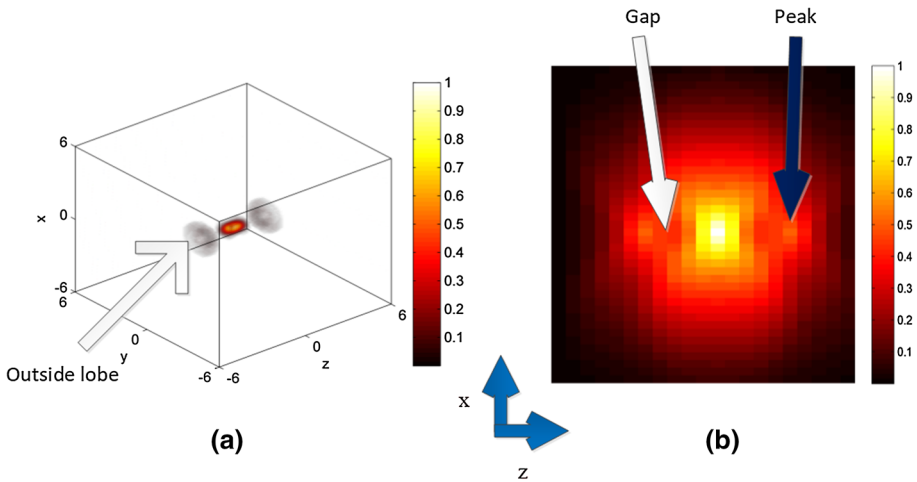


**Fig. 9** The system PSF and MTF in the  $zx$ -plane. The unit along the axis in Fig. 9a is number of wavelengths

sheet fluorescence microscopy, the axial resolution is only along  $z$ -axis ( $z$ -axis—the vertical direction). Therefore, in this paper, we use the asymmetrical type of annular phase mask along the vertical direction to control the shape of the intensity distribution of the doughnut system PSF. The system PSF of the subtraction method can be presented by

$$PSF_{\text{system-sub}}(x, y, z) = PSF_{\text{system1}}(x, y, z) - \beta PSF_{\text{system2}}(x, y, z) \tag{5}$$

where  $\beta$  is the subtraction coefficient and  $PSF_{\text{system1}}$  and  $PSF_{\text{system2}}$  are the system PSFs for the double-beam aperture light sheet and the doughnut light sheet, respectively.

In order to obtain this phase mask, we perform the optimization of the phase mask under the condition: The system PSF of the doughnut light sheet,  $\beta PSF_{\text{system2}}$ , is the nearest with the outside lobes of system PSF of the double-beam aperture beam light sheet,  $PSF_{\text{system1-outside}}$ . Based on this condition, a square error sum of  $PSF_{\text{system1-outside}} - \beta PSF_{\text{system}}$  is used for optimization and an optimal function can be expressed by:

$$\left\{ \begin{array}{l} \text{Min}_{r_i, \beta} \sum \sum \sum |PSF_{\text{system1-outside}}(x, y, z) - \beta PSF_{\text{system2}}(x, y, z)|^2 \\ i = 1, \dots, N; r_i \geq 0.5r \end{array} \right. \tag{6}$$

where  $N$  is the integer and  $r$  is the maximum radius.

Based on the use of optimization function shown in Eq. 6, which can be optimized by the genetic algorithm [23, 24], one optimal phase mask is shown in Fig. 10a and  $\beta = 0.15$ . The PSF of the doughnut light-sheet beam is depicted in Fig. 10b.

The subtraction system PSF is indicated in Fig. 11a. It can be seen that the outside lobes of the system PSF along  $z$ -direction are removed. This means that the gaps in the OTF can be eliminated. In order to highlight it, the MTF in  $zx$ -plane is shown in Fig. 11b. As can be seen from Fig. 11b, there only is one peak in the MTF in  $zx$ -plane. This means that the gaps on the OTF are corrected. In order to clearly show the fitting between the outside lobes of system PSF of the double-beam aperture beam light sheet and the system PSF of the doughnut light sheet, a line profile of the subtraction system PSF along  $z$ -axis is shown in Fig. 11c. It can be seen that the outside lobes of system PSF are removed. This means that there is one good fitting between the outside lobes of system PSF of the double-beam aperture beam light sheet and the system PSF of the doughnut light sheet.



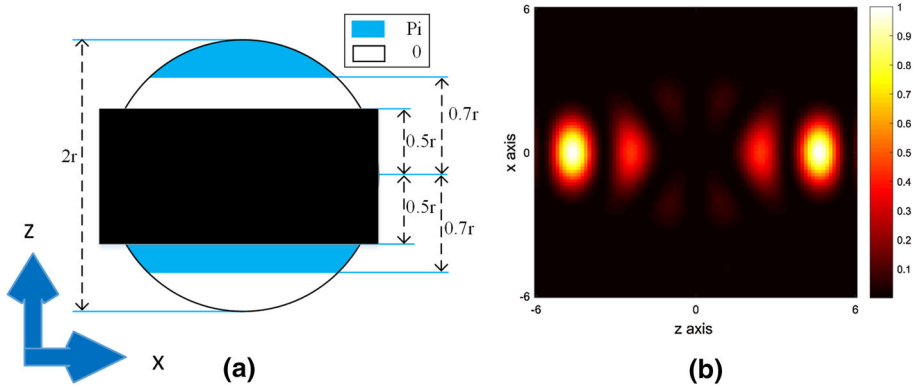


**Fig. 10** The phase mask added optical system. **a** The phase mask, white color is set to 0 and blue color is set to pi. **(b)** The intensity distribution. The unit along the axis in (b) is number of wavelengths

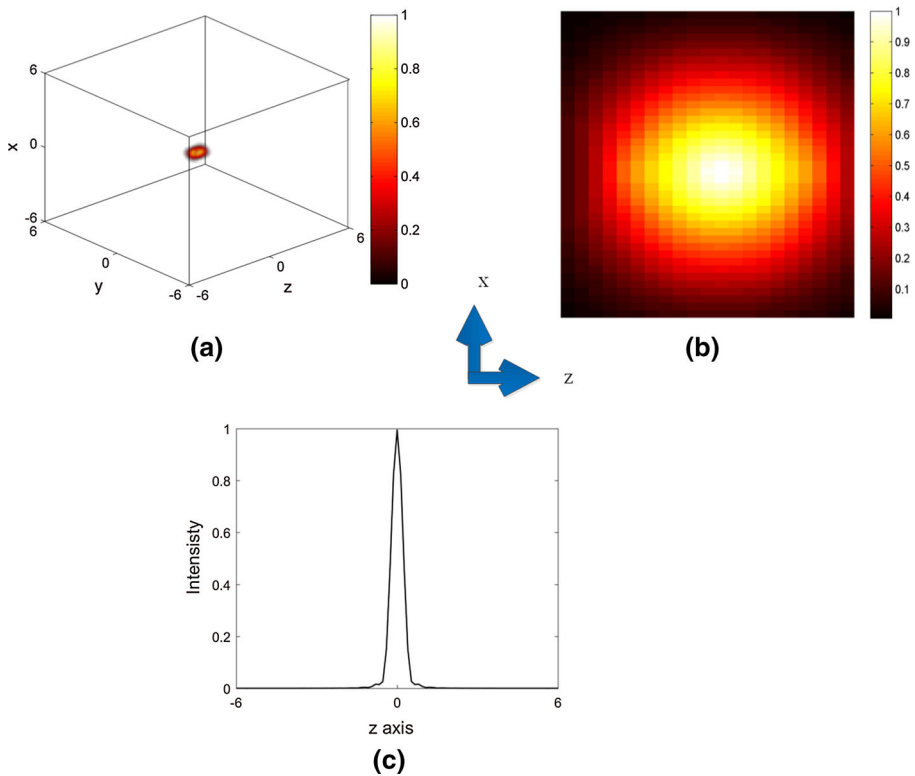


**Fig. 11** The system PSF **a** and MTF **b** in the  $zx$ -plane for the subtraction method. **c** A line profile in  $z$ -axis of the subtraction system PSF

In order to highlight the proposed method, we present the simulation image to prove the effectiveness of this way. The image,  $g$ , can be presented by

$$g = o * \text{PSF} + n \tag{7}$$

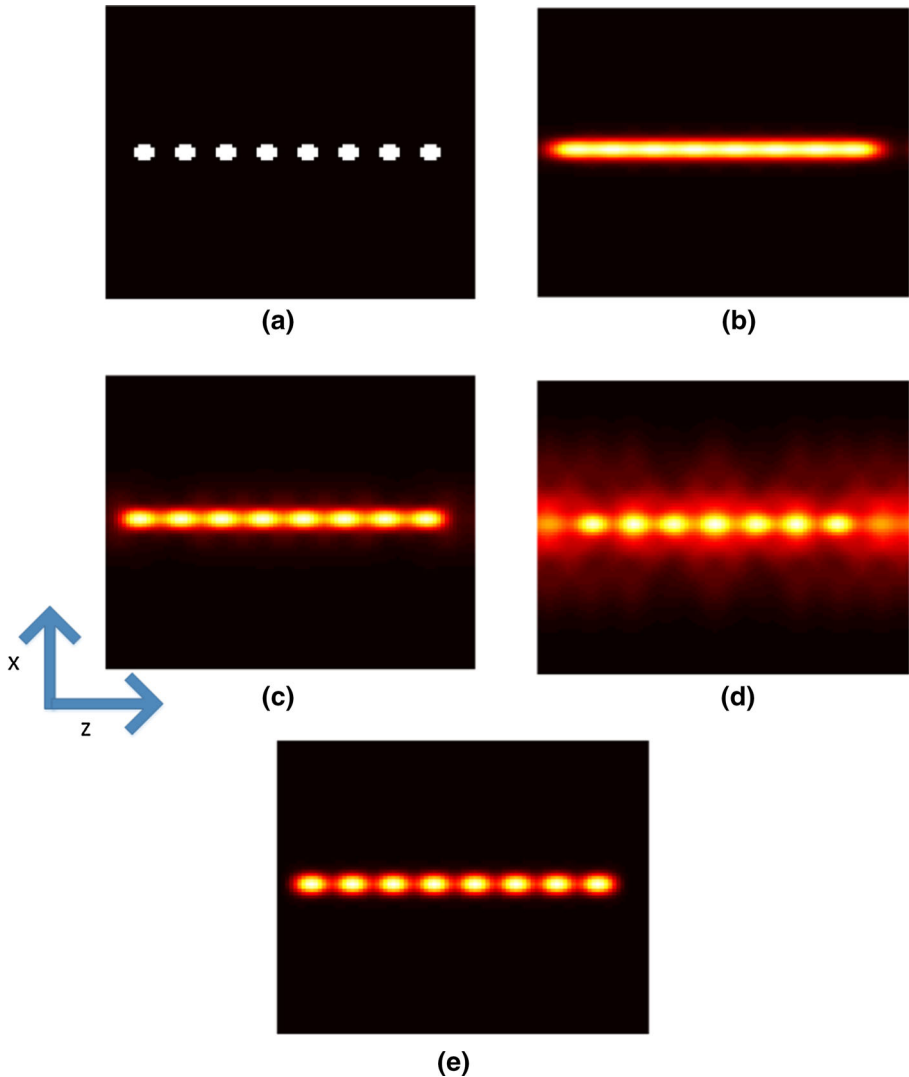


**Fig. 12** Simulation images in the  $xz$ -plane: **a** the original image; **b** the Gaussian light sheet; **c** the double-beam aperture beam light sheet; **d** the doughnut light sheet; **e** the subtraction method

where  $o$  is the object;  $n$  is the noise; and symbol  $*$  is the convolution operation.

Herein, we show the images in  $xz$ -plane. The original image which is used to perform image simulation is indicated in Fig. 12a. Figure 12b–e predicts the simulation images in  $xz$ -plane for the Gaussian light sheet, the double-beam aperture beam light sheet, the doughnut light sheet and the subtraction method, respectively. It is not difficult to see that the axial resolution in  $z$ -axis of both the double-beam aperture beam light sheet and the subtraction method is better than that of the Gaussian light sheet. However, the image of the double-beam aperture beam light sheet still has a disadvantage that the background caused by the outside lobes which are not completely eliminated as indicated in Fig. 12c, while this problem has been avoided in the image of the subtraction method as shown in Fig. 12e.

## 4 Conclusion

In this paper, we have presented one novel, simple method based on the use of pupil function engineering to enhance both axial resolution and field of view of light-sheet fluorescence microscopy. Both NAs of the illumination and detection lenses of 0.3 and 1.1, respectively, are used to demonstrate the effectiveness of the proposed method. The simulation results demonstrated that the double-beam aperture beam light sheet can be used to acquire the remarkable improvement in the axial resolution about 1.2 times in comparison with conventional Gaussian light sheet. The double-beam aperture beam light sheet has a thinner thickness of 1.3 times and longer length with a factor of 1.4 times in comparison with the Gaussian beam light sheet. In other words, the double-beam aperture beam light sheet can be used to achieve the longer length and thinner thickness in comparison with conventional light-sheet fluorescence microscopy. Moreover, we have proposed an effective method to eliminate the outside lobes of the system PSF of the double-beam aperture beam light sheet.

**Acknowledgement** This work is supported by Vietnam National Foundation for Science and Technology Development (NAFOSTED) under Grant Number (103.03-2018.08).

## References

1. H. Siedentopf, R. Zsigmondy, Visualization and size measurement of ultramicroscopic particles, with special application to gold-colored ruby glass. *Ann. Phys.* **10**, 1–39 (1903)
2. A.H. Voie, D.H. Burns, F.A. Spelman, Orthogonal-plane fluorescence optical sectioning: three-dimensional imaging of macroscopic biological specimens. *J. Microsc.* **170**(3), 229–236 (1993)
3. P.J. Keller, A.D. Schmidt, A. Santella, K. Khairy, Z. Bao, J. Wittbrodt, E.H.K. Stelzer, Fast, high-contrast imaging of animal development with scanned light sheet based structured illumination microscopy. *Nat. Method.* **7**, 637–642 (2010)
4. O.E. Olarte, J. Andlla, D. Artigas, P. Loza-Alvares, Decoupled illumination detection in light sheet microscopy for fast volumetric imaging. *Optica.* **2**(8), 702 (2015)
5. H. Dodt, U. Leischner, A. Schierlön, N. Jährling, C.P. Mauch, K. Deininger, J.M. Deussing, M. Eder, Q. Ziegglänsberger, K. Becker, Ultramicroscopy: three-dimensional visualization of neuronal networks in the whole mouse brain. *Nature Method.* **4**, 331–336 (2007)
6. P.J. Keller, A.D. Schmidt, J. Wittbrodt, E.H.K. Stelzer, Reconstruction of Zebrafish early embryonic development by scanned light sheet microscopy. *Science* **332**, 1065–1069 (2008)
7. E. Fuchs, J.S. Jaffe, Thin laser light sheet microscopy for microbial oceanography. *Opt. Express* **10**(2), 145 (2002)
8. K. Mohan, S.B. Purnapatra, P.P. Mondal, Three dimensional fluorescence imaging using multiple light sheet microscopy. *PLoS ONE* **39**, 4715 (2014)
9. L. Silvestri, A. Bria, L. Sacconi, G. Lannello, F.S. Pavone, Confocal light sheet microscopy: micron-scale neuroanatomy of entire mouse brain. *Opt. Express* **18**, 20482–20598 (2012)
10. J. Huisken, J. Swoger, F.D. Bene, J. Wittbrodt, E.H.K. Stelzer, Optical sectioning deep inside live embryos by selective plane illumination microscopy. *Science* **305**, 1007 (2004)
11. A.K. Gustavsson, P.N. Petrov, M.Y. Lee, Y. Shechtman, W.E. Moerner, 3D single-molecule super-resolution microscopy with a tilted light sheet. *Nat. Commun.* **9**(123), 1 (2018)
12. R. Itoh, J.R. Landry, S.S. Hamann, O. Solgaard, Light sheet fluorescence microscopy using high-speed structured and pivoting illumination. *Opt. Lett.* **41**(21), 5015–5018 (2016)
13. C. Gohn-Kreuz, A. Rohrbach, Light sheet generation in inhomogeneous media using self-reconstructing beams and the STED-principle. *Opt. Express* **24**(6), 5855 (2016)
14. V. Le, X. Wang, C. Kuang, X. Liu, Axial resolution enhancement for light sheet fluorescence microscopy via using the subtraction method. *Opt. Eng.* **57**(10), 103107 (2018)
15. L. Gao, L. Shao, B.-C. Chen, E. Betzig, 3D live fluorescence imaging of cellular dynamics using Bessel beam plane illumination microscopy. *Nat. Protocols.* **9**(5), 1083–1101 (2014)
16. T. Vetterburg, H.I.C. Dalgarno, J. Nytk, C. Coll-Llado, D.E.K. Ferrier, T. Czmar, F.J. Gunn-Moore, K. Dholakia, Light sheet microscopy using an Airy beam. *Nat. Methods* **11**, 541–544 (2014)

17. M. Friedrich, Q. Gan, V. Ermolayev, G.S. Harms, STED-SPIM: stimulated emission depletion improves sheet illumination microscopy resolution. *Biophys. J.* **100**(8), L43–L45 (2011)
18. Z.T. Zhao et al., Multicolor 4D fluorescence microscopy using ultrathin Bessel light sheets. *Sci. Rep.* **6**(26159), 1 (2016)
19. B.J. Chang et al., Light-sheet engineering using the field synthesis theorem. *J. Phy. Photonics* **2**(1), 014001 (2019)
20. R. Elena et al., How to define and optimize axial resolution in light-sheet microscopy: a simulation-based approach. *Biomed. Opt. Express* **11**, 8–26 (2020)
21. V. Le, X. Wang, C. Kuang, X. Liu, Background suppression in confocal scanning fluorescence microscopy with superoscillations. *Opt. Commun.* **426**, 541–546 (2018)
22. P. Gao, G. Ulrich Nienhaus, Precise background subtraction in stimulated emission double depletion nanoscopy. *Opt. Lett.* **42**(4), 831–834 (2017)
23. H.T. Liu, Y.B. Yan, G.F. Jin, Design and experimental test of diffractive superresolution elements. *Appl. Opt.* **45**, 95–99 (2006)
24. N.B. Jin, Y.R. Samill, Advances in particle swarm optimization for antenna designs: real-number, binary, single-objective and multi-objective implementations. *IEEE Trans. Antennas Propag.* **55**, 556–567 (2007)